Developing Algorithmic Machinery to Explore the Cosmological Horizon Problem by Numerically Solving Maxwell's Equations in the Kasner Metric

Elizabeth Wu

Abstract

The Horizon Problem posits the cosmological question: if the early universe was not homogenous to begin with, and information cannot travel faster than the speed of light, how could the Cosmic Microwave Background (CMB) be at such a uniform temperature everywhere? The Mixmaster model of the universe posits that the early universe "churned" to evenly distribute matter and radiation, exhibiting repeated chaotic, oscillating Kasner epochs alternating between an expanding and contracting universe at different rates in different directions. Unlike prior studies involving the Kasner metric, this study modeled light as a wave rather than rays, allowing it to retain significant physical properties. The purpose of this study was to numerically find electromagnetic wave speed from the physically interesting Kasner case, in order to model early universe light behavior. Algorithms in Wolfram Mathematica were written to numerically solve Maxwell's equations in this metric for propagation speed, as there is no known analytical solution. To test this simulation program, the light-ray expectation of the velocity of the models was compared to results produced by waves, demonstrating successful development of a calculation tool to gain insight into the Horizon Problem. Numerically determined results from a light-wave model matched those of a ray, while algorithms were developed to address improperly orthonormalized functions that present a "contaminating" standing wave. As expected, results support the hypothesis: numerically determined wave speeds match those produced by ray tracing, suggesting that a calculation tool has been developed in order to explore further Kasner cases in a non-vacuum universe.

1. Introduction

1.1 The Early Universe and the Cosmic Microwave Background

Beginning as an initial singularity of apparently infinite density and temperature, the early universe can be described by the Big Bang Theory, but there are still uncertainties about its earliest phases. (Guth, 2000)

Evidencing the occurrence of the Big Bang, the Cosmic Microwave Background (CMB) is remnant electromagnetic radiation from the early universe produced by the decoupling of photons from hot plasma, when photons were able to travel long distances for the first time in the universe's history. This occurred because photons were emitted when electrons combined with protons to form hydrogen atoms, during a period of the universe's expansion and cooling. These photons are still traveling today, and are observed as microwaves in the CMB. (Spergel and Zaldarriaga, 1997)

1.2 The Horizon Problem

The CMB shows that the universe is isotropic (uniform with respect to angle) and homogenous (uniform with respect to position), as the average CMB is a steady 2.726 ± 0.001 K throughout the entire sky. Consider an observer at any point in the universe examining opposite ends of the horizon (Figure 1). The view from the two ends of the observable universe demonstrates that light from opposite sides of the CMB has traveled 13 billion light-years to reach the observer. However, Einstein's Theory of Special Relativity establishes that no information can travel faster than the speed of light in a vacuum. Thus, it can be said that these opposites ends were outside of each other's horizons when the light was emitted from either area, meaning that the universe has not existed long enough for information traveling at the speed of light to connect these two regions, so there is a difficulty in explaining the apparent homogeneity of the CMB across causally disconnected areas in space. (Guth, 1981)

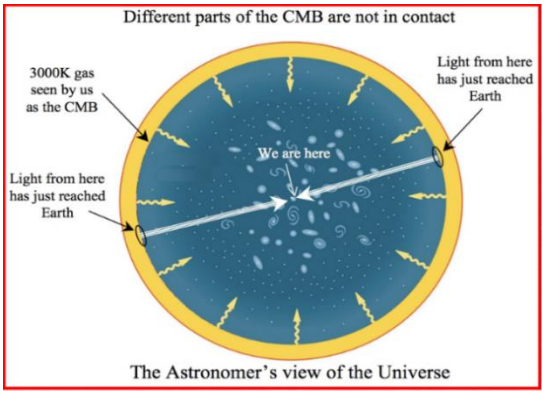

Figure 1. Areas from opposite ends of the observable universe are too far apart to have communicated, so they are "causally disconnected". (Whittle, 2008)

The evenness of the CMB poses the cosmological problem: areas in the universe too far apart to have communicated without violating causality appear to be in equilibrium. Since the universe was not initially homogenous, how could the CMB be at such a uniform temperature? (Brandenberger, 2000)

The inflationary model is a common attempt to solve the Horizon Problem by proposing that there was a 10^{-36} second epoch after the Big Bang Singularity during which exponential expansion allowed for the universe to equilibrate in temperature. However, this paradigm is ambiguous, as the physical mechanics behind inflation are unknown and unproven. For example, no inflatons (hypothetical inflation particles theorized to drive inflation), or signs in the CMB of primordial gravitational waves ("B-Modes") have been observed. (Akrami et al., 2019)

1.3 The Kasner Metric and Mixmaster Universe

Positing that there was a chaotic epoch where the early universe "churned" to evenly distribute matter and radiation, the Mixmaster Universe is Misner's (1969) solution to Einstein's field equations of General Relativity. Modelling oscillating intervals of the universe's expansion, the Mixmaster Universe describes growing and shrinking across three dimensions of space. This may have allowed for distant regions of space to come in contact with each other, so the early universe was able to achieve the homogeneity observed in the CMB. (Pettini, 2018)

Each of these chaotic, oscillating epochs can be described as exhibiting Kasner behavior, as the Mixmaster model consists of an infinite number of Kasner epochs, alternating between an expanding and contracting universe at different rates in different directions. To solve Einstein's field equations for gravitational behavior in this model, the Kasner metric is a function that defines spacetime interval *ds* in a vacuum as a function of time *t* as follows: (Brevik and Pettersen, 1997):

$$ds^2 = -c^2\,dt^2 + t^{2p_x}\,dx^2 + t^{2p_y}\,dy^2 + t^{2p_z}\,dz^2 \qquad \text{(Equation 1).}$$

The Kasner exponents must satisfy the following conditions:

$$p_x + p_y + p_z = 1 \text{ and } p_x^2 + p_y^2 + p_z^2 = 1 \qquad \text{(Equations 2, 3).}$$

The two interesting sets of integer solutions to Equations 2 and 3 are:

$$(0, 0, 1) \text{ and } \left(\frac{2}{3}, \frac{2}{3}, -\frac{1}{3}\right) \qquad \text{(Equation 4).}$$

These solutions are significant because they exhibit cylindrical symmetry in spacetime, because two indices are the same, resulting in symmetry across two axes of space.

However, previous work involving the Kasner metric typically assumed a restrictive simplification by approximating light as rays, rather than as waves. For a ray-tracing approximation (geometrical optics approximation), $ds^2 = 0$, and solving for $\frac{dx}{dt}$, $\frac{dy}{dt}$, and $\frac{dz}{dt}$ provides the light-ray propagation speeds. Instead, this study models light as waves rather than rays, allowing it to retain physical properties such as diffraction. (Montani et al., 2008)

1.4 EM Propagation and the Kasner Metric

Serving as the foundations for classical electromagnetism, Maxwell's equations describe the unifying relationships between electricity and magnetism. (Maxwell, 2013)

The electromagnetic wave equations in vacuum space can be derived from Maxwell's equations. However, Maxwell's equations are usually written for flat spacetime (in the absence of gravity), so they must be applied to the curved-space Kasner metric. Assuming that there is no medium to conduct charges, zero is substituted for both charge and current in Maxwell's equations. After making this substitution and using vector field operations and identities, the result is a second-order partial differential equation, which could be further simplified because symmetry results from two of the Kasner exponents being equal (Equation 4).This gives the time-dependent differential equation of the electric or magnetic field $F_i(t)$ in the direction normal to the plane of symmetry, where k_x, k_y, k_z are defined as the electromagnetic wave vector and overdots are time derivatives (Bochner 2015):

$$\left[(t^{-2p_x})k_x^2 + (t^{-2p_y})k_y^2 + (t^{-2p_z})k_z^2\right]F_i(t) + \left(\frac{p_i}{t}\right)\dot{F}_i(t) + \ddot{F}_i(t) = 0 \qquad \text{(Equation 5).}$$

Since $p_x = p_y$ in both Kasner cases (Equation 4), the x-y plane is the plane of symmetry, so $F_i(t)$ is in the z-direction (e.g., the z-component of the vector field *F*). Applying the Kasner metric (Equation 1) with the $(p_x, p_y, p_z) = (0, 0, 1)$ exponent case to the 4-dimensional wave equation (Equation 5) in spacetime results in the following modification to Equation 5:

$$\frac{1}{c^2}\ddot{F}_z(t) + \frac{1}{t}\dot{F}_z(t) + \left(k_x^2 + k_y^2 + \frac{k_z^2}{t^2}\right)F_z(t) = 0 \qquad \text{(Equation 6)}$$

However, the *(0, 0, 1)* Kasner case is physically trivial and does not give insight into the Horizon Problem because the *x* and *y* components are constant if the p_x and p_y exponents are 0, and z is directly proportional to time *t* because the p_z exponent is 1. As a result, it can be shown that this case does not represent expanding spacetime.

On the other hand, applying Kasner metric (Equation 1) with the $(p_x, p_y, p_z) = (\frac{2}{3}, \frac{2}{3}, -\frac{1}{3})$ exponent case results in:

$$\frac{1}{c^2}\ddot{F}_z(t) - \frac{1}{3t}\dot{F}_z(t) + \left(\frac{k_x^2+k_y^2}{t^{\frac{4}{3}}} + t^{\frac{2}{3}}k_z^2\right)F_z(t) = 0 \qquad \text{(Equation 7)}$$

More complex and interesting physics can be derived from Equation 7; its solutions resembling Bessel functions (oscillating functions associatied with cylindrical waveguides), but unfortunately, Equation 7 has no known exact analytical solution. Thus, the study will focus numerically finding solutions to Maxwell's equations in this physically interesting Kasner metric case.

2. Purpose and Hypothesis

The purpose of this study is to numerically find solutions to the equation from the physically significant *(2/3, 2/3, -1/3)* Kasner case, in order to model the propagation speed of light waves in the early universe.

It is hypothesized that, to test this study's simulation program, the light-ray expectation of the velocity of the models will match the result produced by a light wave model. This demonstrates the successful development of a calculation tool, which will be extended to another model with radiation-filled cosmology in future work, prospected to reveal unforeseen properties of light as waves that deviate from properties attributed to light as rays.

3. Methodologies

Algorithms in Wolfram Mathematica Version 11.3 were written to conduct the numerical programs. All procedures were first used on the following differential equation:

$$\frac{d^2y}{dt^2} = -y \qquad \text{(Equation 8)}$$

Equation 8 was used as a simple test differential equation because it has well known solutions of sines and cosines. Afterwards, the same procedures were conducted on the more complicated Equation 7, where the constant speed of light in a vacuum was set as $c = 1$ to simplify calculations.

3.1 Orthonormalizing Functions

Two solutions to the second-order differential equation of form Equation 8 were found using the `NDSolve` function, and initial conditions were varied so that the solution functions would not necessarily be orthogonal. This was to show that orthogonality can be found numerically, which will later be used on the more complex solutions to Equation 7. One of the solutions, *f(t)*, was normalized so that:

$$\int_{t_n}^{t_{n+2}} f(t)^2 = 1 \qquad \text{(Equation 9)}$$

across one period. The period was found by finding a zero *n*, and finding the second zero *n+2* that occurred after *N*.

Then, a second solution to the differential equation, $g_0(t)$ was modified with the following integral, to produce orthogonalized function $g(t)$:

$$g(t) = g_0(t) - \int_{t_n}^{t_{n+2}} f(t)g_0(t) \qquad \text{(Equation 10)}$$

This resulted in orthogonality such that:

$$\int_{t_n}^{t_{n+2}} f(t)g(t) = 0 \qquad \text{(Equation 11)}$$

Then, $g(t)$ was normalized using the same process applied to *f(t)*. All integration was performed numerically using the `NIntegrate` function.

3.2 Defining the Wave Function and the Wavefront

The two orthonormalized functions, *f(t)* and $g(t)$, were combined to form the wave function:

$$w(t) = f(t)\cos(k_i x + \phi_R) + g(t)\sin(k_i x + \phi_R) \quad \text{(Equation 12)}$$

As introduced in Equation 5, k_i is the component of wave vector (k_x, k_y, k_z) in the direction that the wave is propagating. For simplicity, this study defined the magnitude of k_i to be 1. Then, to define a wavefront at *w(0) = 0*, the phase shift ϕ_R was solved to be:

$$\phi_R = \tan^{-1}(-\frac{f(0)}{g(0)}) \quad \text{(Equation 13)}$$

3.3 Propagating the Wavefront

To propagate the wavefront forwards, the wavefront *x(t)* was defined as a function of time, based on the wave equation (Equation 12):

$$x(t) = \frac{1}{k_i}(\tan^{-1}\left(-\frac{f(t)}{g(t)}\right) - \phi_R) \quad \text{(Equation 14)}$$

Since $tan^{-1}(t)$ is a discontinuous function that "resets" every period π, a periodic step function $Q\pi$ was added to Equation 14 to ensure that it would propagate forwards, where Q would increment by one, starting at zero, every time *x(t)* encountered a discontinuity. As a result, the propagating wavefront is produced:

$$x(t) = \frac{1}{k_i}(\tan^{-1}\left(-\frac{f(t)}{g(t)}\right) - \phi_R) + Q\pi \quad \text{(Equation 15)}$$

The wavefront function *x(t)* was manipulated by defining *x(t)* as a list of values, with a step size of $\Delta t = 0.0001$.

3.4 Finding Wave Velocity

To find wave velocity, the derivative of Equation 15 was numerically approximated by iteratively taking the following:

$$x(t) = \frac{x(t+\Delta t) - x(t)}{\Delta t} \quad \text{(Equation 16)}$$

Due to machine limitations, to ensure that Equation 16 was calculated within a reasonable time frame, this study used $\Delta t = 0.0001$. Then, the result was plotted along with the predicted velocity produced from ray tracing (ie., solving Equation 1 for $\frac{dx}{dt}$, $\frac{dy}{dt}$, and $\frac{dz}{dt}$ when $ds^2 = 0$).

Afterwards, residuals were plotted to precisely show deviations from the ray prediction, using the equation:

$$Residual = speed_{wave} - speed_{ray} \quad \text{(Equation 17).}$$

4. Results and Discussions

4.1 Sinusoidal Work

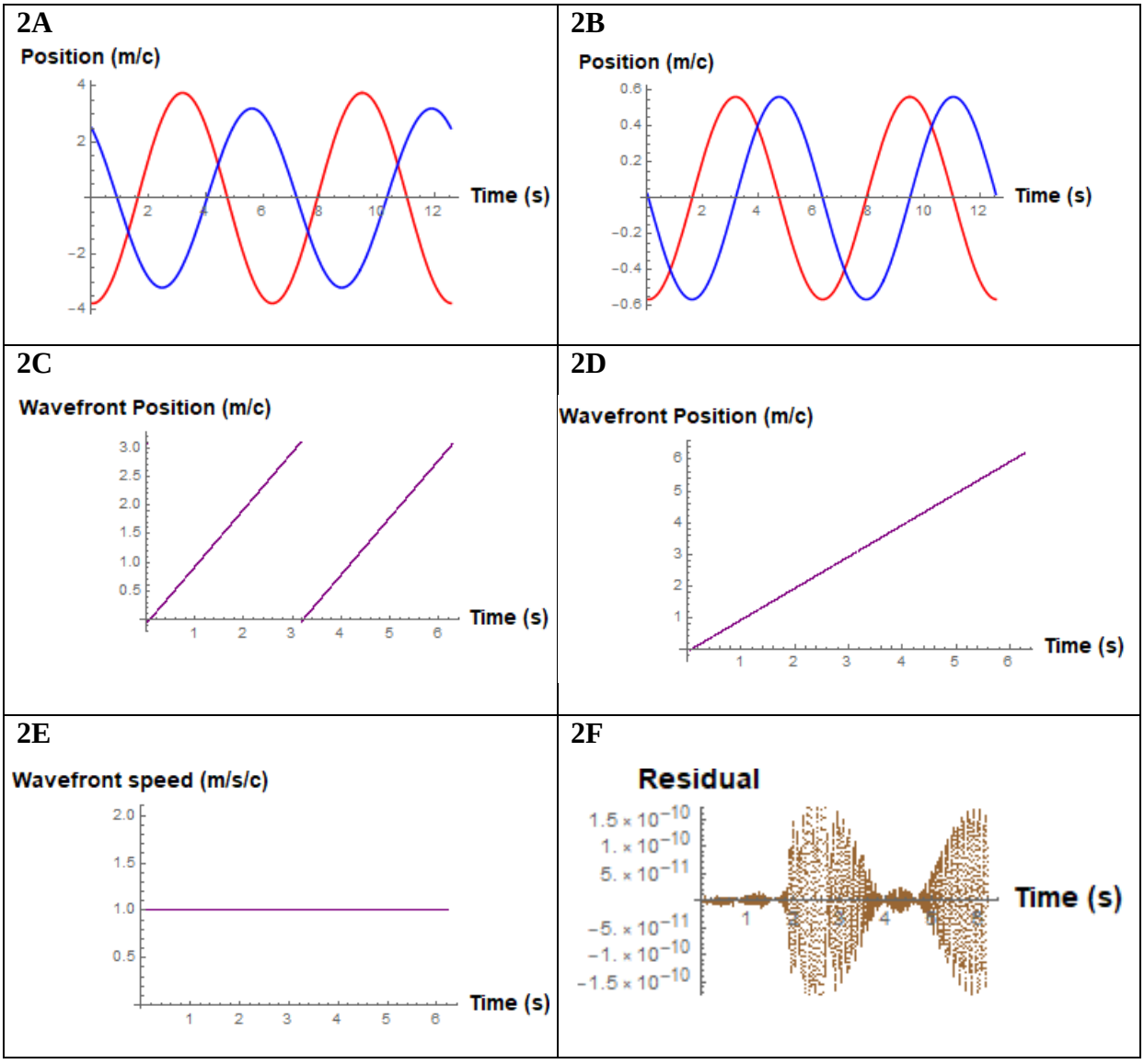

Figures 2A & 2B. Functions before and after orthonormalization. **Figure 2C.** The wavefront, modeled by Equation 14, is discontinuous when propagated forwards because it contains an inverse tangent function, which is periodic to phase π. **Figure 2D.** Propagating the wavefront of the simpler, sinusoidal functions produces a smooth, linear curve after the discontinuities are corrected (Equation 15). **Figure 2E.** Since *c* was set to equal 1 in all calculations, wave speed equals one in this case, which matches the light-ray predicted value of one. **Figure 2F.** The

difference between the experimentally determined wave speed and ray predicted wave speed was graphed as residuals. (All 6 figures generated by competition entrant)

4.1.1 Modeling the Wavefront

Functions *f(t)* (red) and $g(t)$ (blue), graphed in Figure 2A, are solutions to two different differential equations. When the functions are normalized properly, a purely propagating wavefront, without any standing wave, should be constructed. After *f(t)* and $g(t)$ are orthonormalized (Figure 2B), they are combined in Equation 12 to produce a wave, whose wavefront is then propagated forwards via Equation 17, demonstrated by Figure 2C. It is worth noting that all results have been divided by a factor of *c,* the speed of light, because this study set the constant *c = 1* (such as in Equation 7) for simplicity, so the y-axis on all figures are "per unit *c"*.

4.1.2 Phase Velocity

Correcting the propagated wavefront fixes the discontinuities, producing a smooth curve (Figure 2D), whose derivative gives the velocity of the wavefront. Taking the derivative (Figure 2E) produces the wave velocity. The small residuals of -11 orders of magnitude (Figure 2F) suggests that the errors occur from loss of some numerical precision in the software, signaling that the mathematically machinery built was successful and the study can proceed to evaluate the Bessel-like equations (Equation 7).

4.1.3 Correcting for Improperly Normalized Functions and Demonstrating the "Contaminating" Standing Wave

In the case of improperly normalized functions, where there are unbalanced amounts of *f(t)* or $g(t)$ in wave Equation 12, oscillating phase velocities were observed. The simpler, sinusoidal functions that had been normalized were "un-normalized" by introducing a factor *A* into the wave equation such that:

$$w(t) = f(t)\cos(k_i x + \phi_R) + A * g(t)\sin(k_i x + \phi_R) \qquad \text{(Equation 18)}$$

This is because it is difficult to perfectly normalize Bessel-like functions numerically due to their non-constant periods, so the behavior of improperly normalized wave functions was first demonstrated in simple sinusoidal functions.

A correcting factor *B* was introduced such that:

$$w(t) = f(t)\cos(k_i x + \phi_R) + B * A * g(t)\sin(k_i x + \phi_R) \qquad \text{(Equation 19)}$$

Starting at 1, the value of *B* was varied to show that, as *B* approached $\frac{1}{A}$, the experimentally determined wavefront speed would approach the speed predicted by ray tracing (Figures 3A -D).

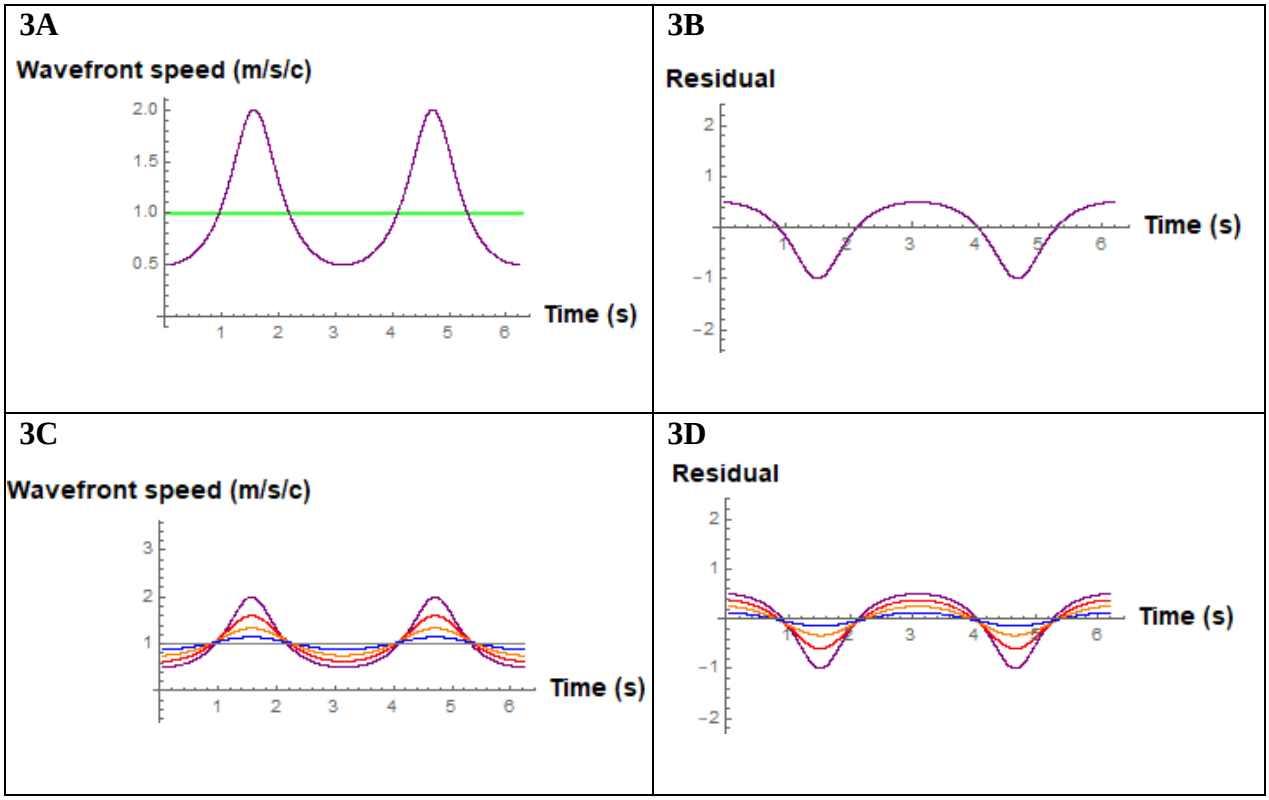

Figure 3A. Wavefront speed from improperly normalized functions (purple) when *A = 0.5* and *B = 1* plotted against the predicted speed (green). **Figure 3B**. Oscillating residuals from the curve in Figure 3A. **Figures 3C & D.** Purple, red, orange, blue, and gray curves *show B = 1.0, 1.25, 1.5, 1.75, 2.0* respectively, when *A = 0.5*. It is worth noting that *B = 2.0* produced a residual that matched Figure 2F precisely. (All 4 figures generated by competition entrant)

Since *f(t)* and $g(t)$ are solutions to the second order differential Equation 8 (which produces sinusoidal solutions), and the process of normalization produces a factor α that is the same for both *f(t)* and $g(t)$ such that their amplitudes are equal, they can be written as the following:

$$f(t) = \alpha \cos(t) \text{ and } g(t) = \alpha \sin(t) \quad \text{(Equation 20 and 21)}$$

The oscillations of wave functions containing improperly normalized *f(t)* and $g(t)$ can be attributed to the presence of a "contaminating" standing wave. This can be shown as such: substituting Equations 20 and 21 and into the wave Equation 12 produces the following (wave vector *k* has been set to 1 for simplicity):

$$w(t) = \alpha * \cos(t)\cos(x + \phi_R) + \alpha * \sin(t)\sin(x + \phi_R) \quad \text{(Equation 22)}$$

When the functions are improperly normalized, there is some contaminating factor β such that there are uneven amounts of *f(t)* and $g(t)$.

$$w(t) = \alpha * \cos(t)cos(x + \phi_R) + (\alpha - \beta) * \sin(t)\sin(x + \phi_R) \quad \text{(Equation 23)}$$

Factoring $(\alpha - \beta)$ out of the righthand side of Equation 23 produces the sum of a purely propagating wave function and a standing wave.

$$w(t) = (\alpha - \beta)[\cos(t)\, cos(x + \phi_R) + \sin(t)\sin(x + \phi_R)] + \beta \cos(t) \cos(x + \phi_R)$$

(Equation 24)

Since $(\alpha - \beta)$ is the factor for both the cosines and sines in Equation 23, the expression

$$(\alpha - \beta)[\cos(t) \cos(x + \phi_R) + \sin(t)\sin(x + \phi_R)]$$

represents a properly normalized, purely propagating wave. This is because applying the cosine angle-sum formula to the expression above produces the following wave that only propagates rightwards as *t* increases:

$$(\alpha - \beta)[\cos(t) \cos(x + \phi_R) + \sin(t)\sin(x + \phi_R)] = (\alpha - \beta)\cos[t - (x + \phi_R)] \quad \text{(Equation 25)}$$

Thus, Equation 24 can be rewritten as:

$$w(t) = (\alpha - \beta)\cos[t - (x + \phi_R)] \; + \beta \cos(t) \cos(x + \phi_R) \quad \text{(Equation 26)}$$

However, the addition of

$$\beta \cos(t)\, cos(x + \phi_R)$$

introduces a standing wave into the function, resulting in the oscillating wave velocities that produce oscillating residuals as well.

4.2 Kasner Work

4.2.1 Modeling the Wavefront

The periods in the more complicated Bessel-like functions were not constant, which may have resulted in imperfect orthonormalization. Two cases were examined: a wave propagating in the x and/or y-direction (Figure 4A), and a wave propagating in the z-direction (Figure 4B). Since periods increases as time continues in a wave propagating in the z-direction, those waves were evaluated over a longer time interval in order to obtain sufficient zeroes for orthonormalization.

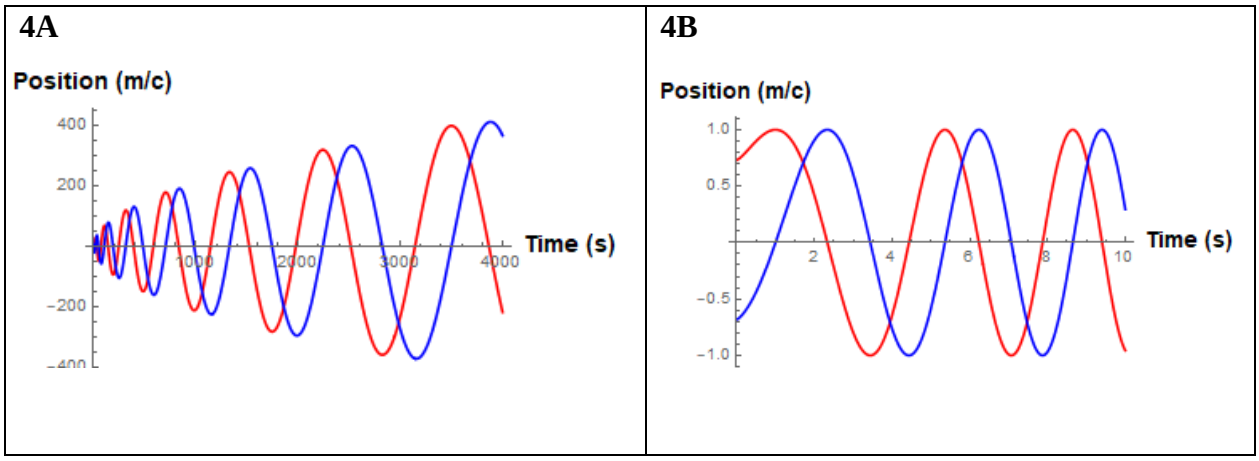

Figure 4A. Orthonormalized Bessel-like functions modeling a wave propagating the x and/or y direction. As time increases, period grows longer. **Figure 4B.** Orthonormalized Bessel-like functions modeling a wave propagating the z direction. As time increases, period grows shorter. (Both figures generated by competition entrant)

Modeling a wave propagating in the x and/or y-direction was achieved by setting the wave vector constants k_x, k_y in Equation 7 to nonzero values (this study used 1, for simplicity) and $k_z$was set to 0. Likewise, in the case of a wave propagating in the z-direction, k_x, k_y were set to 0 and k_z was set to 1. In the equation, k_x and k_y can be combined, resulting in a wave that is propagating in one or both of those directions.

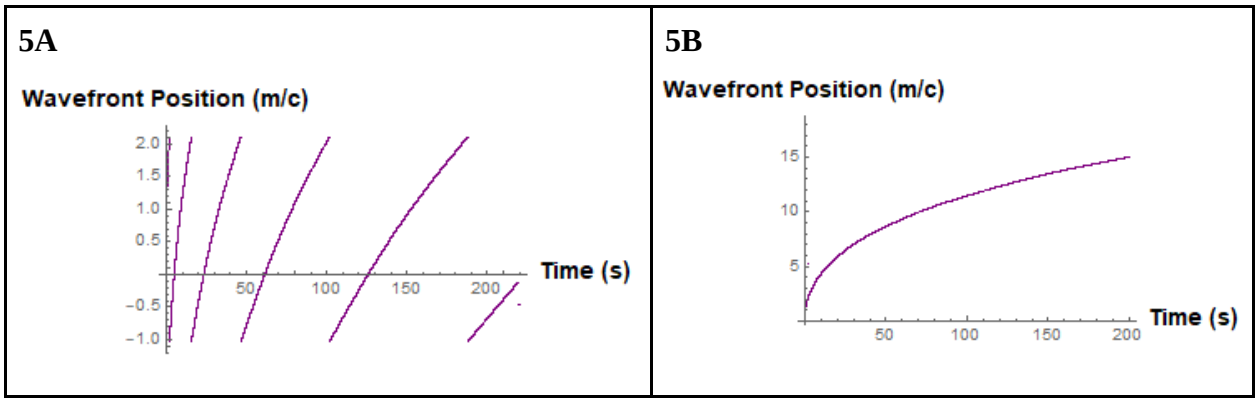

Figures 5A & B. A propagating wavefront in the x and/or y-direction, before and after being corrected for discontinuities. (Both figures generated by competition entrant)

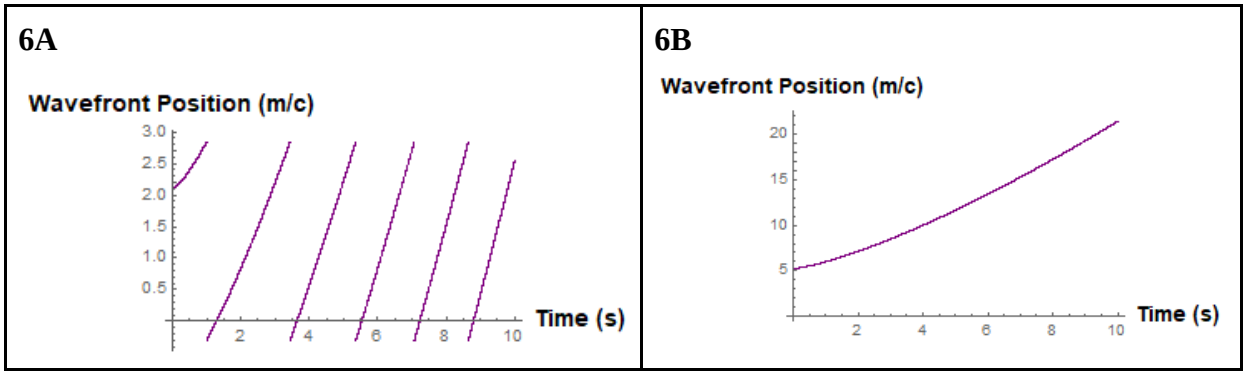

Figures 6A & B. A propagating wavefront in the z-direction, before and after being corrected for discontinuities. (Both figures generated by competition entrant)

4.2.2 Wave Phase Velocity and Comparisons to Ray Predictions

The possible imperfections in orthonormalization, caused by the variable periods, may have led to small deviations between the numerically determined wave speed (purple) and the ray predicted speed (green), as plotted in Figures 7A and 7B. In both of these plots the curves strongly overlap.

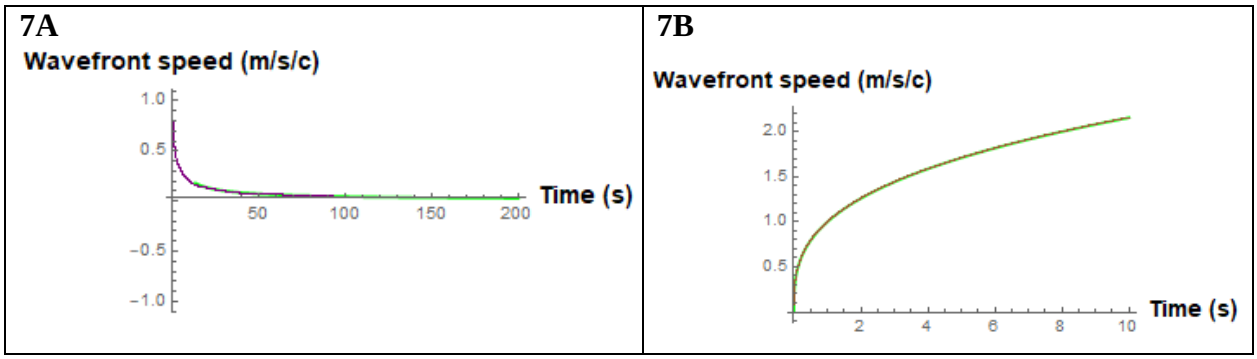

Figure 7A. The speed of the wavefront of a wave propagated in the *x* and/or *y* direction. Modeled as a ray, the light's speed should be: $\frac{c}{t^{2/3}}$. **Figure 7B.** The speed of the wavefront of a wave propagated in the *z* direction. Modeled as a ray, the light's speed should be: $ct^{1/3}$. (Both figures generated by competition entrant)

The oscillating values of the residuals about the x-axis suggests that there is a patterned fluctuation of the numerically determined phase speed around the ray-predicted determined speed (Figures 8A and 8B), indicating the presence of a "contaminating" standing wave in analogy with the sinusoidal case.

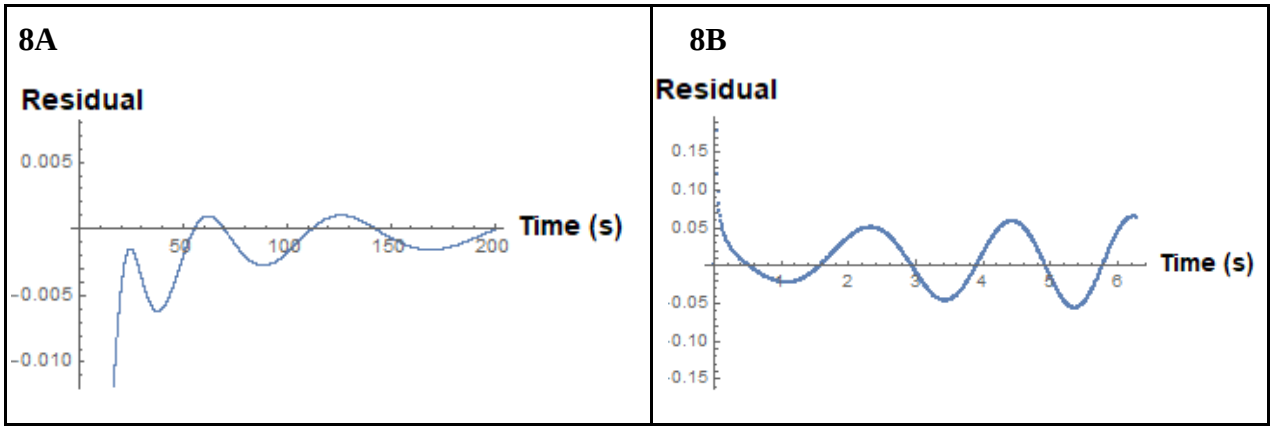

Figure 8A. Residuals for a wave propagating in the x- and/or y-direction. **Figure 8B.** Residuals for a wave propagating in the z-direction. (Both figures generated by competition entrant)

These residuals occur due to the fact that normalization of the Bessel-like functions was imperfect, since they have variable periods, resulting in unbalanced amounts of *f(t)* or $g(t)$ in Equation 12. Thus, the unbalanced quantities of either function allowed for the presence of a standing wave in the wave equation, leading to the small, oscillating errors depicted in Figures 8A and 8B, which can be tuned by varying a correction factor.

4.2.3 Correcting for Improperly Normalized Functions

A correction factor *C* was introduced to the wave equation such that:

$$w(t) = f(t)\cos(kx + \phi_R) + C * g(t)\sin(kx + \phi_R) \qquad \text{(Equation 27)}$$

Starting at 1, the value of *C* was varied by increments of 0.1 to determine whether there was too much or too little of *g(t)* (*C < 1* if too much, *C > 1* if too little), and then it was varied by smaller increments to narrow down the correct value of *A* in order to properly normalize $g(t)$ with respect to *f(t)*.

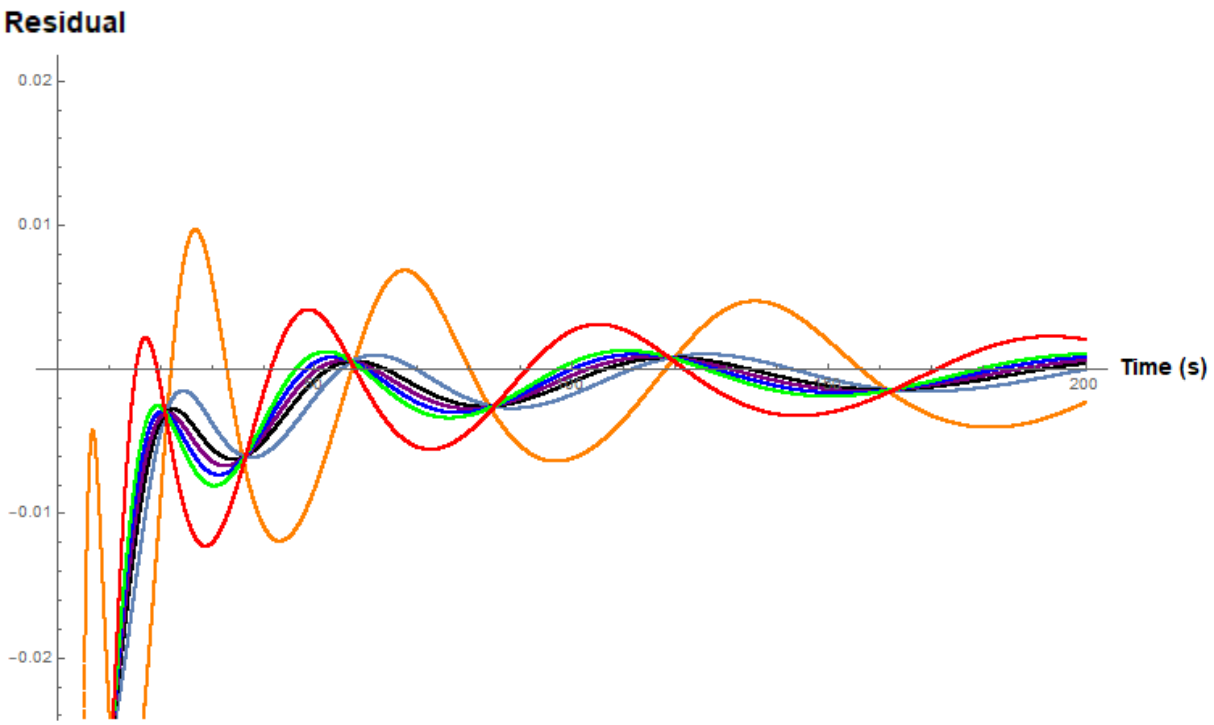

Figure 9. Orange, gray-blue, black, purple, blue, green, and red curves represents residuals produced by *C = 0.9, 1.0, 1.02, 1.03, 1.04, 1.05, 1.1* respectively. (Generated by competition entrant)

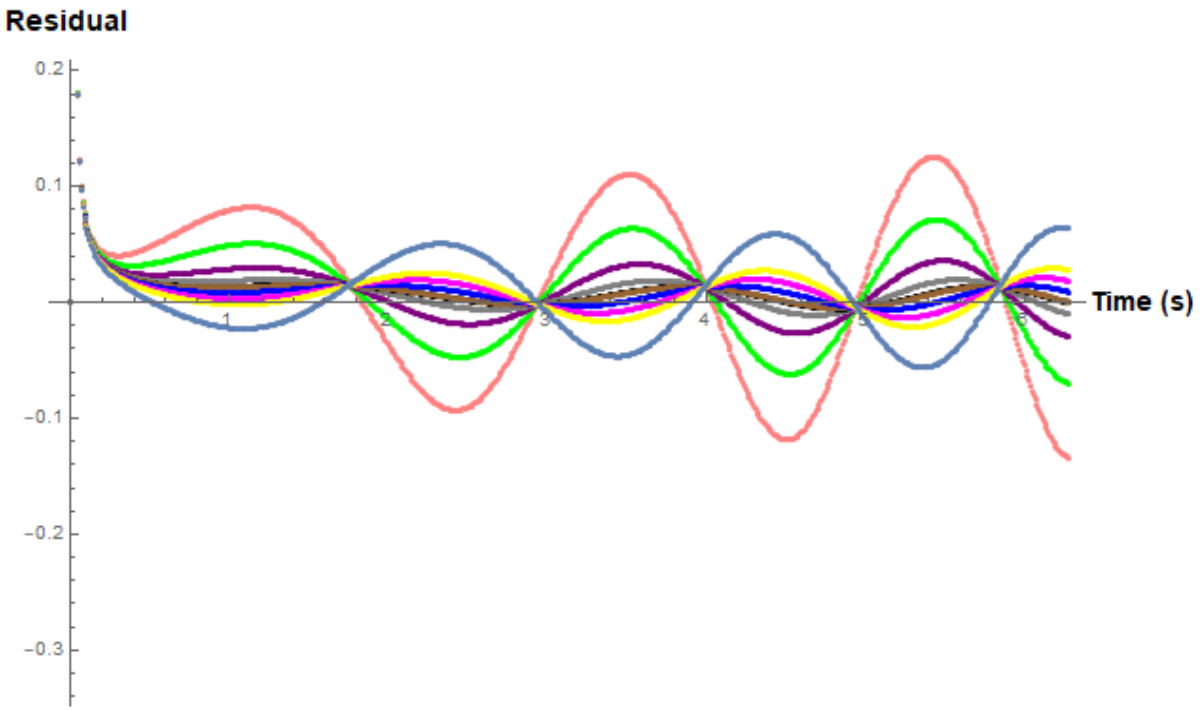

Figure 10. Orange, green, purple, brown, blue, magenta, and yellow curves represents residuals produced by *C = 0.9, 0.93, 0.95, 0.96, 0.97, 0.98, 1.0* respectively. (Generated by competition entrant)

In both the xy-propagating and the z-propagating waves, varying the correction factor reduced the residuals, as the oscillations were flattened as *C* corrected more of the imperfect normalization. Still, as shown by Figures 7A and 7B, it is worth noting that the numerical results closely follow those predicted by ray-tracing.

4.3 Limitations

As shown by the residuals, loss of precision can result from both limits in numerical precision in the software (e.g., roundoff errors and a non-infinitesimal step size), and the nature of the Bessel functions themselves. The former occurs due to limited RAM and preset specifications in Mathematica programming, while the latter, as previously discussed, can be due to imperfect normalization due to the functions' variable periods. As shown by the residuals, numerical errors become more challenging to eliminate as time *t* approaches 0, especially since one of the light-ray predicted curves ($\frac{c}{t^{2/3}}$) is asymptotic to infinity at 0.

5. Conclusions

Developing algorithmic machinery to examine light wave propagation under the *(2/3, 2/3, -1/3)* Kasner case, this study numerically approximated light wave models based on second order differential equations with no known analytical solutions. Unlike prior studies involving the Kasner metric, this study modeled light as a wave rather than rays, allowing it to retain its significant physical properties (such as diffraction). As expected, results support the hypothesis: the numerically determined wave speeds matched those produced by ray tracing, suggesting that a calculation tool has been developed in order to explore further cases in a non-vacuum universe.

6. Future Studies

The *(2/3, 2/3, -1/3)* Kasner metric is directly generalizable to the Kuang-Li-Liang (KLL) metric, which describes a radiation-filled, rather than a vacuum, universe. (Kuang et al., 1987) Solutions to Maxwell's equations in the KLL metric have not yet been found and will be researched in the future. The calculation tools developed by this study will be used to model light waves in that radiation-filled metric once those solutions are found, and it is prospected that the tools developed by this study will uncover new information about light wave behavior that has not been predicted by ray approximations. The early universe was a radiation-dominated era, so this would provide further insight into early behavior of light and clues about the apparent homogeneity of the CMB. Thus, the models in this study will play a role within the broader context of the Horizon Problem and the beginnings of the universe.

Bibliography

Akrami, Ashdown, Aumont, Barreiro, Basak, Bernard, Bersanelli, Bock, Bond, Borrill, Bouchet, Boulanger, Bucher, Butler, Calabrese, Cardoso, Carron, Challinor, Chiang, L. P. L., Combet, Contreras, Crill, De Bernardis, De Zotti, Di Valentino, Diego, Donzelli, Doré, Douspis, Efstathiou, Elsner, Eriksen, Fergusson, Finelli, Franceschi, Frolov, Galli, Ganga, Gauthier, Gerbino, Ghosh, González-Nuevo, Górski, Gratton, Gudmundsson, Hamann, Handley, Hansen, Herranz, Hooper, Huang, Jaffe, Jones, Keihänen, Keskitalo, Kim, Kisner, Krachmalnicoff, Kunz, Lamarre, Lattanzi, Lawrence, M. Le, Lewis, Liguori, Lindholm, Lubin, P. M., and Planck Collaboration. "Planck 2018 Results. X. Constraints on Inflation." *Astronomy and Astrophysics* (2019): n. pag. *ArXiv.org*. ESO Sciences, 02 Aug. 2019. Web. 25 Oct. 2019. <10.1051/0004-6361/201833887>.

Brandenberger, Robert H. “Inflationary Cosmology: Progress and Problems.” *Astrophysics and Space Science Library Large Scale Structure Formation*, vol. 247, 2000, pp. 169–211., doi:10.1007/978-94-011-4175-8_4.

B. Bochner, "Solving the Einstein-Maxwell Equations for the Propagation of Electromagnetic Radiation during Early Universe Kasner-like Epochs", 28th Texas Symposium in Geneva, Switzerland, December 13-18, 2015, https://indico.cern.ch/event/336103/session/7/contribution/82/attachments/1204341/1832967/Proceedings--28_Tex_in_Geneva--Bochner.pdf

B. Bochner, "Electromagnetic Propagation in Anisotropic Kasner Cosmologies and Inhomogeneous, Plane-Symmetric, Radiation-filled metrics", Poster presented at the 22nd International Conference on General Relativity and Gravitation, "Mathematical Relativity and Classical Gravitation" Session (Valencia, Spain, July 7-12, 2019)

Brevik, I., and S. V. Pettersen. “Viscous Cosmology in the Kasner Metric.” *Physical Review D*, vol. 56, no. 6, 1997, pp. 3322–3328., doi:10.1103/physrevd.56.3322.

Guth, Alan H. “Inflationary Universe: A Possible Solution to the Horizon and Flatness Problems.” Physical Review D, vol. 23, no. 2, 1981, pp. 347–356., doi:10.1103/physrevd.23.347.

Guth, Alan H. *The Inflationary Universe: The Quest for a New Theory of Cosmic Origins*. Addison-Wesley Longman, Incorporated, 2000.

Kuang, Zhi-Quan, Jian-Zeng Li, and Can-Bin Liang. "Completion of Plane-symmetric Metrics Yielded by Electromagnetic Fields." *General Relativity and Gravitation* 19.4 (1987): 345-50. Print.

Maxwell, James Clerk. *Dynamical Theory of the Electromagnetic Field*. Martino Fine Books, 2013.

Misner, Charles W. “Mixmaster Universe.” *Physical Review Letters*, vol. 22, no. 20, 1969, pp. 1071–1074., doi:10.1103/physrevlett.22.1071.

Montani, Giovanni, et al. “Classical And Quantum Features Of The Mixmaster Singularity.” International Journal of Modern Physics A, vol. 23, no. 16n17, 2008, pp. 2353–2503., doi:10.1142/s0217751x08040275.

Montani, Giovanni, et al. “Classical And Quantum Features Of The Mixmaster Singularity.” *International Journal of Modern Physics A*, vol. 23, no. 16n17, 2008, pp. 2353–2503., doi:10.1142/s0217751x08040275.

Noble, B. “The Solution of Bessel Function Dual Integral Equations by a Multiplying-Factor Method.” *Mathematical Proceedings of the Cambridge Philosophical Society*, vol. 59, no. 2, 1963, pp. 351–362., doi:10.1017/S0305004100036987.

Pettini, M. “Relativistic Cosmology.” Introduction to Cosmology. 2018, University of Cambridge, Institute of Astronomy.

Spergel, David N., and Matias Zaldarriaga. “Cosmic Microwave Background Polarization as a Direct Test of Inflation.” *Physical Review Letters*, vol. 79, no. 12, 1997, pp. 2180–2183., doi:10.1103/physrevlett.79.2180.

Whittle, Mark. “The Cosmological Framework.” Graduate Extragalatic Astronomy. 2008, University of Virginia, people.virginia.edu/~dmw8f/astr5630/Topic16/t16_horizon_problem.html.